BIBECHANA
Vol. 23, No. 1, January 2026, 93–104

ISSN 2091-0762 (Print), 2382-5340 (Online)
Journal homepage: http://nepjol.info/index.php/BIBECHANA
Publisher:Dept. of Phys., Mahendra Morang A. M. Campus (Tribhuvan University)Biratnagar

Ab initio analysis of structural and physical properties of MgX (X=Ag, Au) alloys

Subash Dahal[1,2], Dev Raj Sapkota[2], Bhupal Guragain[1], Uchit Chaudhary[3] Denisha Khadka[2] , Shashit Kumar Yadav[1]*

[1]*Department of Physics, Mahendra Morang Adarsh Multiple Campus, Tribhuvan University* Biratnagar, Nepal.

[2]*Department of Physics, Damak Multiple Campus, Tribhuvan University* Damak, Jhapa, Nepal.

[3]*Central Department of Physics, Tribhuvan University Kirtipur, Nepal.*

*Corresponding author. Email: sashit.yadav@mmamc.tu.edu.np

Abstract

In this study, we employed first-principles Density Functional Theory (DFT) calculations using the Perdew–Burke–Ernzerhof (PBE) pseudopotential in Quantum ESPRESSO code to investigate the structural, electronic, mechanical, vibrational, and thermodynamic properties of MgAg and MgAu intermetallic compounds. Structural optimizations confirmed that both compounds crystallize in the cubic Tetraauricupride structure with excellent agreement between the calculated lattice constants and available literature. The electronic band structures and projected density of states (PDOS) revealed the metallic nature of both compounds, with distinct orbital contributions near the Fermi level. Mechanical stability was confirmed through elastic constants satisfying the Born-Huang criteria, with MgAu demonstrating higher stiffness, lower compressibility, and slightly greater ductility compared to MgAg. Phonon dispersion relations and density of states confirmed the dynamical stability of both compounds, showing positive phonon frequencies across the Brillouin zone. Thermodynamic analyses, including vibrational free energy, entropy, heat capacities, and the Grüneisen parameter, indicated that MgAu exhibits enhanced thermal stability and stronger thermal expansion effects. The consistency between results obtained from phonon density of states and Brillouin zone integration further validates the accuracy of the predictions. These findings provide valuable insights into the potential applications of MgAg and MgAu alloys in areas such as materials design, catalysis, and electronic devices.

Keywords
Quantum ESPRESSSO, Density Functional Theory, elastic constant, thermodynamics properties, electronic properties.

Article information
Manuscript received: June 10, 2025; Accepted: August 1, 2025
DOI https://doi.org/10.3126/bibechana.v23i1.83384

1 Introduction

Alloys constitute the majority of the materials used in today's technological world. Understanding atomic structure and bonding, the local arrangement of atoms, and their crystal structures is essential for explaining and predicting how materials are processed, characterized, and perform [1,2]. Alloys are among the most important materials that have successfully met modern technological needs to a considerable extent [3, 4]. Magnesium-based alloys, such as MgAu and MgAg, are of particular interest in applications where a combination of low density and enhanced mechanical properties is required. Alloying magnesium with elements like gold (Au) and silver (Ag) can lead to the formation of strengthening phases that contribute to improved structural performance. These strengthening phases typically develop through processes of solid-state nucleation and growth, which enhance the overall strength and stability of the alloy. MgAu and MgAg alloys offer the potential for lightweight materials with superior strength-to-weight ratios, making them promising candidates for advanced engineering applications [5–7].

A considerable amount of research has been conducted on MgAg alloys at ambient pressure to investigate their structural, electronic, mechanical, dynamical, and thermodynamic characteristics [7]. Besterci et al. assessed the electrical conductivity of MgAg alloys with different Mg contents that had been internally oxidized [6]. Liu et al. explored the valence band electronic structures of these alloys using a combination of ultraviolet and X-ray photoelectron spectroscopies, alongside first-principles calculations for band structure and photocurrent properties [8]. Chouhan et al. conducted a detailed analysis of the structural, electronic, mechanical, and phonon properties of MgAg through first-principles approaches [9]. Liu et al. examined the stable and metastable compositions and structures of the MgAg system using a variable composition evolutionary algorithm and first-principles calculations [10]. Other studies focused on the impact of pressure on the structural, mechanical, dynamical, and thermodynamic properties of MgAg using density functional theory [7].

Over the last few decades, binary MgAg alloys have become the subject of much attention due to their potential use in high-temperature structural applications. These alloys are known for their exceptional resistance to corrosion in oxidizing environments at elevated temperatures [5]. The structural, electronic, and phonon properties of MgAg in the cesium-chloride phase have been examined using density functional theory (DFT) within the local density approximation (LDA) framework [9]. Chouhan et al. investigated the structural characteristics of CsCl-type binary intermetallic compounds of gold and silver with rare-earth metals using X-ray diffraction methods [9]. Ferro et al. summarized the alloying behavior and stability of gold, silver, and copper, drawing from both experimental data and literature [4]. Curtarolo et al. studied the structural stability of binary intermetallic compounds using *ab initio* theory within the LDA/GGA (local density approximation/generalized gradient approximation) methods [3].

While substantial research has been devoted to understand the structural stability and mechanical properties, there has been limited focus on the detailed investigation of temperature variation of mechanical and thermodynamic properties and comparison of structural, electronic, vibrational, mechanical, and thermodynamic properties of MgAg and MgAu compounds. This gap in research has prompted us to undertake a systematic investigation of these properties in the present study.

2 Computational details

In this work, first-principles calculations were conducted within the framework of density functional theory (DFT) using the Quantum ESPRESSO simulation package [11]. The exchange-correlation interactions were treated using the generalized gradient approximation (GGA) with the Perdew-Burke-Ernzerhof (PBE) functional [12]. To accurately model the electron-ion interactions, ultrasoft pseudopotentials were utilized. A plane-wave basis set with a carefully optimized kinetic energy cutoff was employed to ensure convergence and computational accuracy. The Brillouin zone was sampled using a Monkhorst-Pack k-point grid, selected to provide precise total energy calculations and reliable structural optimization. Structural relaxation was performed until the residual forces acting on the atoms were reduced below a defined convergence threshold. The mechanical properties, including elastic constants and elastic moduli, were computed using the thermopw package [13] which applies the stress-strain method to extract the complete elastic tensor. The bulk modulus and shear modulus were determined using the Voigt-Reuss-Hill (VRH) averaging scheme, providing insights into the mechanical stability and resistance to deformation of the materials. Phonon calculations were also performed using density functional perturbation theory (DFPT) to investigate the vibrational properties of the compounds. Phonon dispersion curves and phonon density of states were calculated to verify the dynamic stability and to gain a deeper understanding of lattice vibrational behavior, which is essential for thermodynamic analysis.

3 Results and discussion

3.1 Structural properties

MgAg and MgAu both crystallize in the Tetraauricupride structure with a cubic $Pm\bar{3}m$ space group. In these compounds, magnesium atoms are coordinated in a body-centered cubic geometry, each surrounded by eight equivalent noble metal atoms. The relaxed crystal structures of MgAg and MgAu used in this study are shown in Figure 1. We calculated the bond length, equilibrium lattice constant (a), and formation energy of MgAg and MgAu. The obtained values are presented in Table 1.

The formation energy of materials is obtained by the relation [14–18]

$$E_f = \frac{1}{N}\left(E_{\text{tot}} - n_A E_A - n_B E_B\right), \qquad (1)$$

where E_{tot} represents the total energy associated with the geometric optimization of the system, n_A and n_B denote the number of atoms of types A and B in the crystal system, and E_A, E_B are the ground-state energies of each atom.

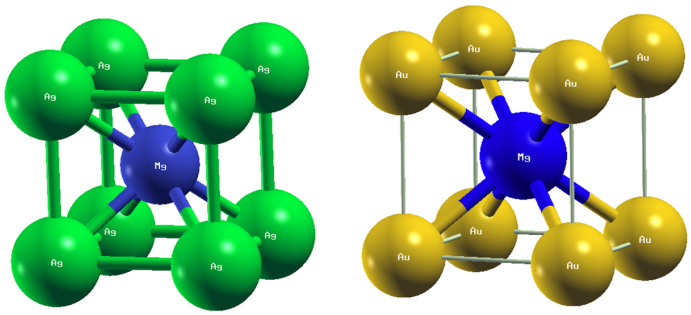

Figure 1: Relaxed crystal structures of MgAg and MgAu alloys.

Table 1: Bond length, lattice constant, and formation energy of MgAg and MgAu alloys.

Compounds	Bond length (Å)	Lattice constant (Å)	Formation energy (eV/atom)
MgAg (This work)	2.8759	3.320	-0.267
Others	–	3.334[a], 3.341[b]	–
MgAu (This work)	2.8602	3.302	-0.622
Others	–	3.312[a]	–

[a] Ref. [9], [b] Ref. [7]

The calculated lattice constant for MgAg is 3.320 Å, which shows good agreement with the previously reported values of 3.334 Å [9] and 3.341 Å [7]. Similarly, the lattice constant for MgAu is calculated to be 3.302 Å, closely matching the literature value of 3.312 Å [9]. The formation energies for MgAg and MgAu are found to be -0.267 eV/atom and -0.622 eV/atom, respectively, indicating that both compounds are thermodynamically stable. The more negative formation energy of MgAu suggests that it is energetically more favorable compared to MgAg.

3.2 Electronic properties

Figure 2(a–d) depict the band structures and projected density of states (PDOS) for MgAg and MgAu alloys, offering valuable insights into their electronic properties. In the band structures (2(a) and 2(b)), the energy dispersion relations for MgAg and MgAu are displayed, respectively. The Fermi level (E_F) is marked at 0 by a solid horizontal line, indicating the energy threshold between occupied and unoccupied states. The band structures reveal the presence of multiple bands crossing or approaching E_F, suggesting metallic behavior for both compounds.

The PDOS plots (2(c) and 2(d)) further dissect the contributions of different atomic orbitals to the total density of states (DOS). For MgAg, the PDOS highlights significant contributions from Mg-s, Mg-p, and Ag-d orbitals near E_F, with the Ag-d states dominating below E_F. This indicates strong hybridization between Mg and Ag orbitals, which could influence bonding and electronic prop-

erties. In contrast, for MgAu, the Au-d states are expected to lie deeper in energy compared to Ag-d, potentially leading to differences in hybridization and electronic behavior. The total DOS near E_F is finite for both compounds, reinforcing their metallic nature.

These findings suggest that both MgAg and MgAu exhibit metallic conductivity, with their electronic properties heavily influenced by the interplay between Mg-(s, p) and noble metal (Ag/Au)-d states. The stronger localization of d-states in MgAu may lead to distinct electronic and bonding characteristics compared to MgAg, which could be relevant for applications in catalysis, spintronics, or alloy design.

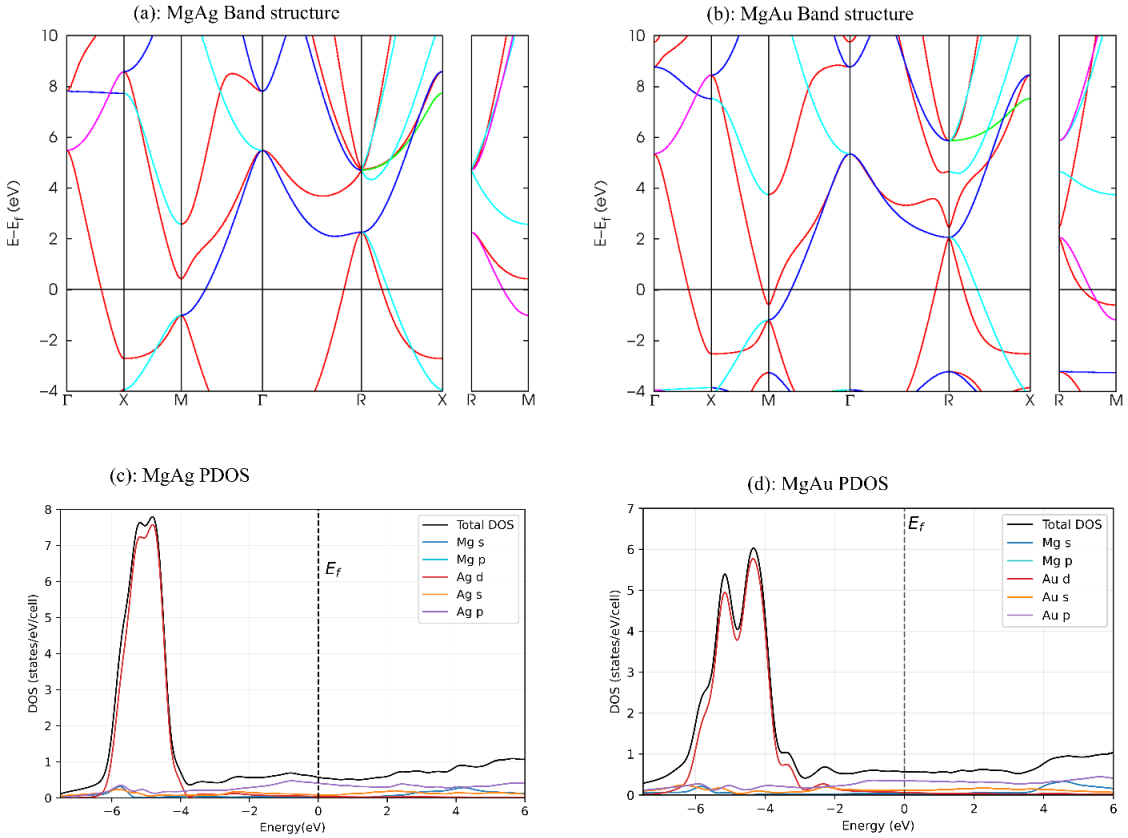

Figure 2: Band structures and PDOS of MgAg and MgAu alloys.

3.3 Vibrational Properties

The phonon band structure and density of states (DOS) provide essential insights into the lattice dynamics, thermal properties, and structural stability of materials. In this work, we have also examined the phonon dispersion relations and DOS for MgAg and MgAu alloys. Figure 3(a-d) shows the phonon band structures and phonon DOS of MgAg and MgAu alloys. These plots reveal how atomic vibrations propagate through the crystal lattice and how their frequencies are distributed in MgAg and MgAu alloys. The phonon analysis shows the absence of imaginary frequencies, which confirms the dynamical stability of the materials [19].

The phonon dispersion relations of MgAg and MgAu demonstrate clear vibrational differences while sharing some fundamental characteristics. Both materials exhibit phonon frequencies extending up to approximately 250 cm^{-1}, with fully positive frequencies throughout the Brillouin zone confirming their dynamical stability. In MgAg (Figure 3(a)), the acoustic branches appear around 100 cm^{-1}, while in MgAu ((Figure 3(b))) they are slightly lower at about 75 cm^{-1}, reflecting the mass difference between Ag and Au atoms. Notably, both systems show a significant separation of about 110 cm^{-1} between their acoustic and optical modes, indicating similar overall gaps in their vibrational spectra. The optical branches in both compounds reach up to the maximum frequency range, with MgAu displaying slightly more dispersed optical modes compared to MgAg. This similarity in overall band structure but difference in specific branch positions highlights how atomic mass affects vibra-

tional properties while maintaining similar qualitative features.

The density of states plots reveal more pronounced differences between the two materials' vibrational characteristics. The MgAg DOS shows a distinctive double peak structure in the lower frequency range (60–90 cm^{-1}), followed by an approximately 80 cm^{-1} gap, and then two well-defined high-frequency peaks at 220 cm^{-1} and 240 cm^{-1}, (Figure 3(c)). In contrast, MgAu presents a more prominent initial peak at 50 cm^{-1} with the same 80 cm^{-1} gap, but develops different high-frequency features with peaks at 180 cm^{-1} and 240 cm^{-1}, (Figure 3(d)). The presence of the gap at nearly similar energies in both materials suggests a common origin in their lattice dynamics, while the varying peak intensities and positions reflect the different atomic masses and bonding environments.

The sharper high-frequency peaks in MgAg indicate more localized vibrational modes compared to MgAu, likely due to the specific arrangement of lighter Ag atoms in the lattice versus the heavier Au atoms. These DOS differences imply potentially distinct thermal and mechanical properties despite their similar maximum frequencies and band gaps.

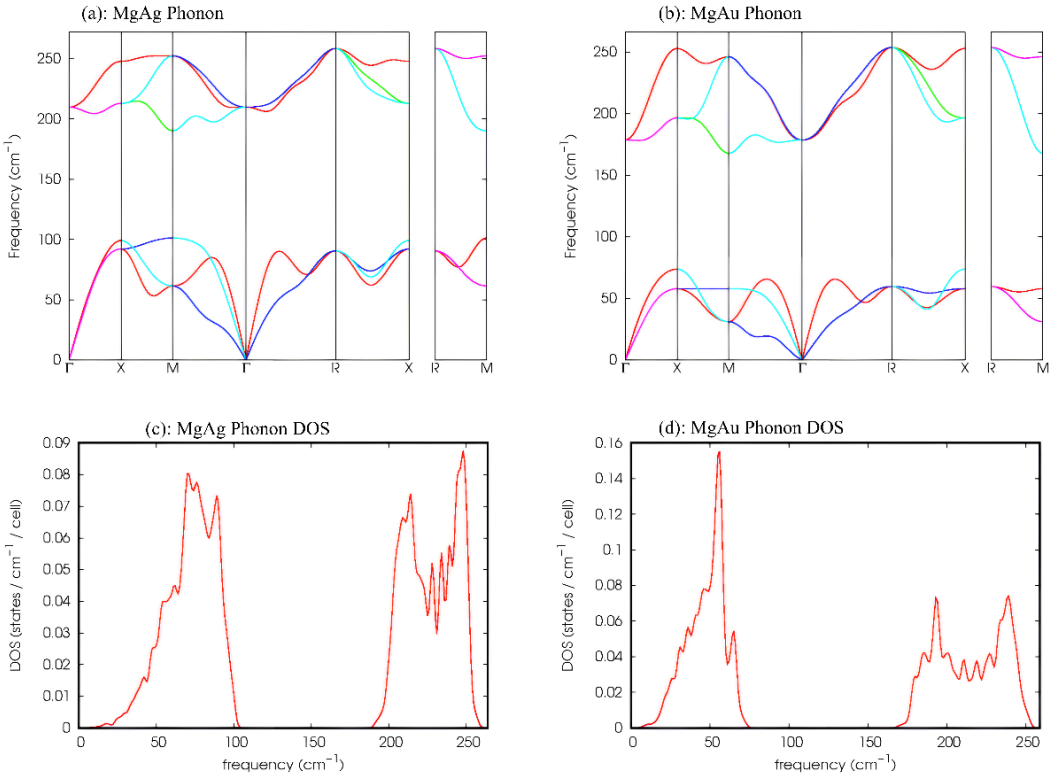

Figure 3: Phonon band structures and phonon density of states (DOS) for MgAg and MgAu alloys.

3.4 Mechanical properties

To gain a deeper understanding of the mechanical properties of the materials, the elastic constant matrices (C_{ij}) were calculated. For the cubic structures of MgAg and MgAu, three independent elastic constants C_{11}, C_{12}, and C_{44} were obtained. These constants were then employed to evaluate the elastic properties through the Voigt–Reuss–Hill (VRH) approximation methods. Based on this approach, the relationships between the bulk modulus (B) and shear modulus (G) can be determined as follows [16, 20–26]

$$B_V = \frac{C_{11} + 2C_{12}}{3}, \tag{2}$$

$$G_V = \frac{C_{11} - C_{12} + 3C_{44}}{5}, \tag{3}$$

$$B_R = B_V, \tag{4}$$

$$G_R = \frac{5(C_{11} - C_{12})C_{44}}{4C_{44} + 3(C_{11} - C_{12})}, \tag{5}$$

$$B = \frac{B_V + B_R}{2}, \quad G = \frac{G_V + G_R}{2}. \tag{6}$$

Furthermore, we calculated the Pugh's ratio (B/G), Young's modulus (Y), Poisson's ratio (ν), and Grüneisen parameter (γ) using the following relations [21, 23, 24]

$$Y = \frac{9BG}{3B+G}, \tag{7}$$

$$\nu = \frac{3B-2G}{2(3B+G)}, \tag{8}$$

$$k = \frac{B}{G}. \tag{9}$$

Table 2 presents a comprehensive comparison of the elastic and mechanical properties of MgAg and MgAu compounds. The listed properties include the elastic constants (C_{ij}), bulk modulus (B), shear modulus (G), Young's modulus (Y), pressure derivatives (B'), Pugh's ratio (k), and Poisson's ratio (ν). These parameters were computed in this study and compared with previously published literature.

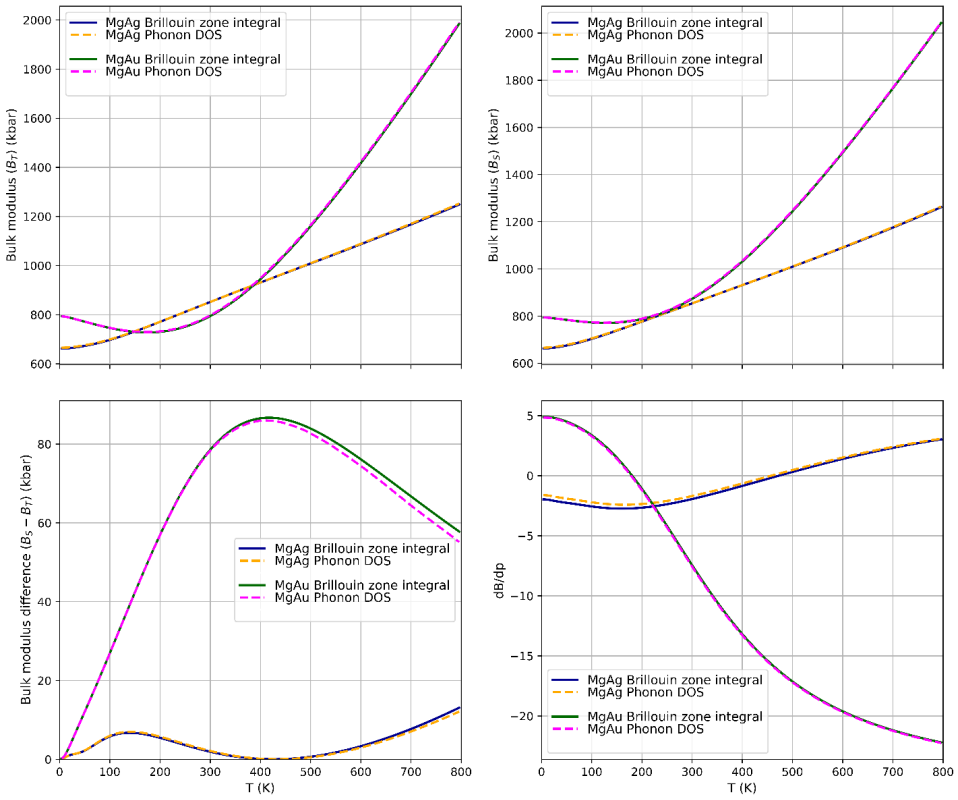

Figure 4: Temperature dependence of (a) isothermal bulk modulus (B_T), (b) isentropic bulk modulus (B_S), (c) their difference $\Delta B = B_T - B_S$, and (d) pressure derivative of bulk modulus (B') for MgAg and MgAu alloys.

The calculated elastic constants (C_{ij}) for MgAg and MgAu confirm their mechanical stability, as they satisfy the Born–Huang stability criteria for cubic crystals [23, 27, 28]. Among the two compounds, MgAu exhibits higher stiffness than MgAg, as evidenced by its larger C_{11} of 102.203 GPa compared to 81.349 GPa for MgAg, indicating stronger resistance to uniaxial deformation. The C_{12} values of 53.832 GPa for MgAg and 71.651 GPa for MgAu suggest that MgAu has greater resistance to shear deformation under compressive stress, while the C_{44} values of 48.691 GPa for MgAg and 50.173 GPa for MgAu indicate that MgAu is slightly more resistant to shear strain. The bulk modulus (B), which represents resistance to volume change, is significantly higher for MgAu (81.835 GPa) than for MgAg (63.005 GPa), indicating that MgAu is less compressible. Similarly, the shear modulus (G), a measure of resistance to shear deformation within the elastic region, is slightly higher for MgAu (31.215 GPa) than for MgAg (29.437 GPa), suggesting marginally better resistance to shape deformation.

Young's modulus (Y), which reflects material stiffness, follows the trend MgAu (82.870 GPa) > MgAg (76.125 GPa), reinforcing that MgAu is mechanically stronger. The Pugh's ratio ($k = B/G$), which distinguishes ductile ($k > 1.75$) from brit-

tle ($k < 1.75$) materials, reveals that both MgAg ($k = 2.140$) and MgAu ($k = 2.621$) exhibit ductile behavior, with MgAu being slightly more ductile. This is further supported by Poisson's ratio (ν), where MgAu ($\nu = 0.327$) shows marginally higher bond flexibility compared to MgAg ($\nu = 0.293$).

These results are consistent with previous studies [7, 9], with minor discrepancies likely attributable to differences in computational parameters, such as the choice of DFT functionals and pseudopotentials. Notably, the calculated C_{44} value for MgAu (50.173 GPa) is lower than the reported literature value of 56.73 GPa, which may result from variations in computational approaches and pseudopotentials used. However, the bulk modulus (B) for both compounds closely matches existing data (Table 2), supporting the reliability of our computational approach.

Table 2: Mechanical parameters of MgAg and MgAu alloys.

Parameter	MgAg (This work)	Others	MgAu (This work)	Others
C_{11} (GPa)	81.349	84.24[a], 85.05[b]	102.203	100.57[b]
C_{12} (GPa)	53.832	55.21[a], 53.26[b]	71.651	74.45[b]
C_{44} (GPa)	48.691	49.59[a], 48.24[b]	50.173	56.73[b]
B (GPa)	63.005	63.85[b]	81.835	83.15[b]
G (GPa)	29.437	30.94[b]	31.215	31.76[b]
Y (GPa)	76.125	79.93[b]	82.870	84.53[b]
B'	4.679	4.673[b]	4.840	4.821[b]
$k = B/G$	2.140	2.063[b]	2.621	2.617[b]
ν	0.293	0.291[b]	0.327	0.330[b]

[a] Ref. [9], [b] Ref. [7]

Furthermore, Figure 4 presents a comparative analysis of the temperature dependence of the bulk modulus and its derivatives for MgAg and MgAu compounds. The plot of isothermal bulk modulus as a function of temperature shows that for both MgAg and MgAu, the bulk modulus initially decreases slightly at low temperatures, reaches a minimum, and then increases significantly with temperature.

Notably, MgAu exhibits a slightly higher bulk modulus than MgAg across the entire temperature range. The plot of the isentropic bulk modulus parameter (B_S) as a function of temperature shows that both MgAg and MgAu display a rising trend in B_S with increasing temperature. The isothermal bulk modulus (B_T) increases more steeply compared to B_S, especially at higher temperatures.

We further calculated and plotted the difference between B_T and B_S, denoted as $\Delta B = B_T - B_S$, as a function of temperature. This difference reflects how the material's resistance to compression changes when considering temperature-dependent effects beyond the static approximation. The observed trend shows that ΔB increases with temperature, reaching a maximum around 400–500 K, and then gradually decreases at higher temperatures. This indicates that the additional thermal effects influencing the bulk modulus are most pronounced in the mid-temperature range and diminish as temperature continues to rise. Furthermore, MgAu consistently exhibits a larger ΔB compared to MgAg across the entire temperature range, suggesting that the compressibility of MgAu is more sensitive to these thermal influences.

We finally calculated the pressure derivative of the bulk modulus (B') as a function of temperature. For MgAg, the derivative starts at negative values at low temperatures and becomes positive at higher temperatures. In contrast, MgAu exhibits the opposite behavior, with B' starting positive at low temperatures and becoming negative as temperature increases. This trend signifies a complex relationship between pressure and bulk modulus under thermal expansion.

The close agreement between the results obtained from Brillouin zone integration and those derived from phonon DOS methods confirms the reliability and accuracy of our computational approach.

3.5. Thermodynamic properties

3.5.1. Helmholtz free energy

Figure 5 presents the computational results related to the Helmholtz free energy. For MgAg, the Helmholtz free energy ranges from approximately −420.98 Ry to −421.03 Ry, whereas for MgAu it ranges from approximately −240.40 Ry to −240.45 Ry. These values indicate the stability of the systems under different configurations or conditions [29]. The results suggest that the phonon contributions to the free energy are significant and vary

with temperature or other parameters. Additionally, the excellent agreement between the two computational methods, namely Brillouin zone integration and phonon DOS, in the temperature range 0–800 K emphasizes the reliability of the results.

3.5.2. Thermal energy, Vibrational free energy, and Entropy

Figure 6 illustrates the thermodynamic properties such as thermal energy, vibrational free energy, and entropy of MgAg and MgAu as functions of temperature, calculated using both the Brillouin zone integration and phonon DOS methods.

The thermal energy increases smoothly with rising temperature for both MgAg and MgAu, following an almost linear trend at higher temperatures. Across the entire temperature range, MgAu consistently exhibits slightly higher thermal energy compared to MgAg, indicating that MgAu absorbs more vibrational energy per mole as the temperature increases.

The vibrational free energy decreases steadily with increasing temperature in both compounds, which is the expected behavior due to enhanced lattice vibrations at elevated thermal states. MgAu consistently shows lower vibrational free energy compared to MgAg, suggesting that MgAu is thermodynamically more favorable at higher temperatures.

Similarly, the entropy increases rapidly at low temperatures and then more gradually at higher temperatures, consistent with the expected population of vibrational degrees of freedom. MgAu displays higher entropy than MgAg across the full temperature range, implying that the vibrational states of MgAu contribute more significantly to the disorder of the system.

The close agreement between the Brillouin zone integration and phonon DOS results validates the reliability of the computational approaches.

3.5.3. Grüneisen parameter, isochoric and isobaric heat capacities

Figure 7 presents the Grüneisen parameter, isochoric heat capacity (C_v), isobaric heat capacity (C_p), and the difference between C_p and C_v as functions of temperature for MgAg and MgAu, calculated using both the Brillouin zone integration and phonon DOS methods. Both compounds show a rapid decrease in the Grüneisen parameter with temperature, particularly at low T, after which the values stabilize.

MgAu consistently exhibits higher Grüneisen parameters than MgAg across the entire temperature range, indicating greater sensitivity of MgAu to volume changes under thermal excitation.

As expected, C_v increases sharply at low temperatures and gradually levels off toward the Dulong–Petit limit [30] at high T. For both compounds, MgAu displays higher C_v values, suggesting that MgAu can store more thermal energy at constant volume.

The behavior of C_p mirrors that of C_v, with MgAu maintaining higher values throughout. The difference $C_p - C_v$ reflects the material's thermal expansion and compressibility. For MgAu, the difference increases with T, peaks around 300–400 K, and then decreases at higher T. For MgAg, the difference shows a smaller variation, with slight increases and decreases before rising again at elevated temperatures. Overall, MgAu consistently shows a larger $C_p - C_v$ difference, indicating stronger thermal expansion effects. Both computational methods yield nearly overlapping trends, underscoring the reliability of the results.

4 Conclusion

In this work, we carried out first-principles calculations to explore the structural, electronic, mechanical, and thermodynamic properties of MgAg and MgAu compounds. The outcomes of our Density Functional Theory (DFT) calculations were carefully analyzed and compared with existing literature to ensure the reliability of our results.

The calculated lattice constants and bond lengths closely match reported values, validating the accuracy of our computational approach. The more negative formation energy of MgAu indicates that it is energetically more stable than MgAg. The band structures and projected density of states (PDOS) confirm the metallic nature of both compounds, as multiple bands cross the Fermi level. The phonon dispersion relations and phonon density of states (DOS) further verify their dynamical stability, with all phonon frequencies remaining positive throughout the Brillouin zone. Both compounds share similar phonon spectra, extending up to approximately 250 cm^{-1} and exhibiting a distinct acoustic–optical gap of about 110 cm^{-1}.

Elastic constant calculations show that both MgAg and MgAu satisfy the Born–Huang stabil-

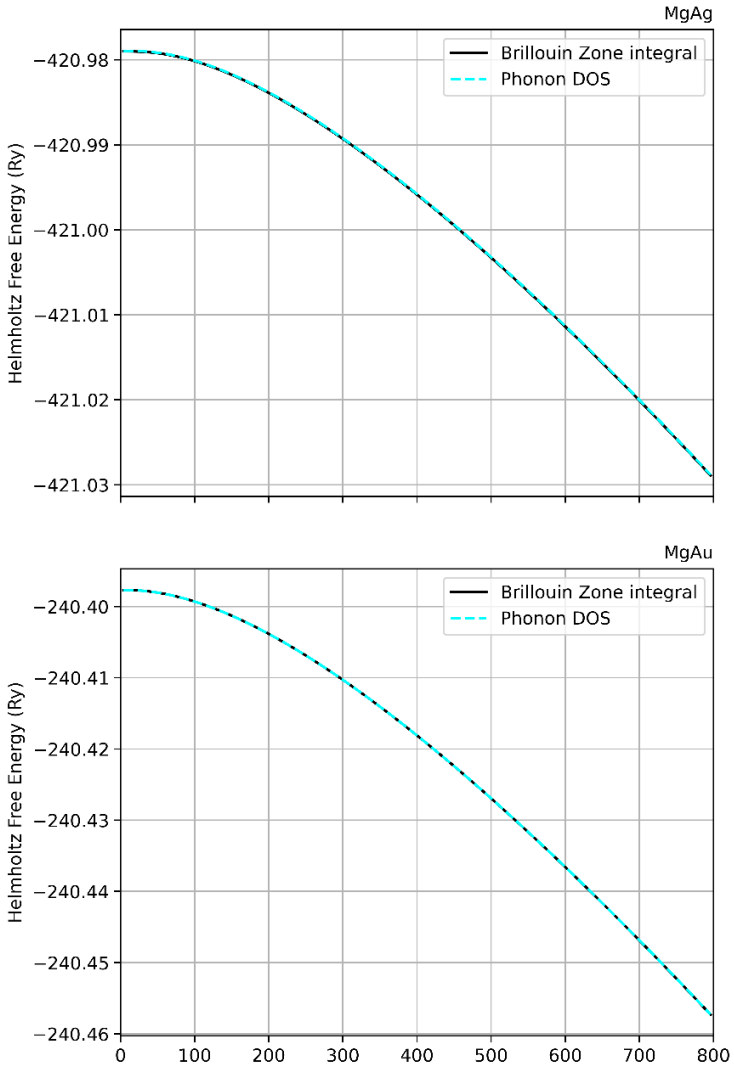

Figure 5: Helmholtz free energy of MgAg and MgAu alloys as a function of temperature.

ity criteria, confirming their mechanical stability. Among the two, MgAu consistently exhibits higher stiffness, greater resistance to deformation, and lower compressibility than MgAg, as reflected by its larger elastic constants, bulk modulus, shear modulus, and Young's modulus. Both alloys demonstrate ductile behavior, as indicated by Pugh's ratio and Poisson's ratio, with MgAu showing slightly higher ductility and bond flexibility.

Thermodynamic analyses reveal that both compounds are stable across a wide temperature range. The Helmholtz free energy confirms their stability under varying conditions, while thermal energy, vibrational free energy, and entropy display consistent temperature dependence. MgAu generally exhibits higher thermal energy, lower vibrational free energy, and greater entropy compared to MgAg, suggesting enhanced vibrational activity and superior thermodynamic favorability. The Grüneisen parameter decreases with temperature, with MgAu showing higher sensitivity to volume changes. Both isochoric (C_V) and isobaric (C_P) heat capacities increase with temperature and saturate at high temperatures, with MgAu consistently exhibiting higher values. The difference between C_P and C_V indicates stronger thermal expansion effects in MgAu.

Overall, the results demonstrate that MgAg and MgAu alloys are structurally, mechanically, and thermodynamically stable, with MgAu consistently outperforming MgAg in terms of energetic favorability, stiffness, ductility, and thermal response. Across all properties, the Brillouin zone integration and phonon DOS methods produce highly consistent results, confirming the robustness and reliability of our computational predictions.

References

[1] S. D. Griesemer, L. Ward, and C. Wolverton. High-throughput crystal structure solu-

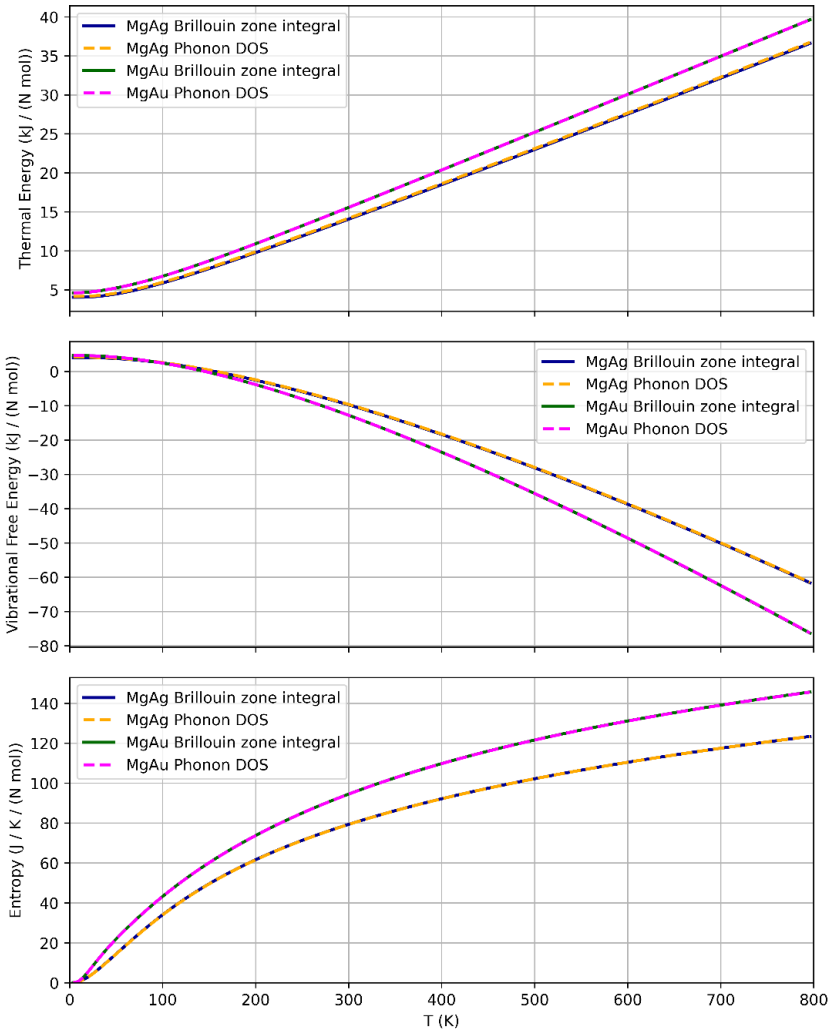

Figure 6: Thermal energy, vibrational free energy, and entropy of MgAg and MgAu alloys as a function of temperature.

tion using prototypes. *Physical Review Materials*, 5(10):105003, 2021.

[2] T. Bucko, J. Hafner, S. Lebègue, and J. G. Angyan. Improved description of the structure of molecular and layered crystals: ab initio dft calculations with van der waals corrections. *The Journal of Physical Chemistry A*, 114(43):11814–11824, 2010.

[3] S. Curtarolo, D. Morgan, and G. Ceder. Accuracy of ab initio methods in predicting the crystal structures of metals: A review of 80 binary alloys. *Calphad*, 29(3):163–211, 2005.

[4] R. Ferro, A. Saccone, D. Maccio, and S. Delfino. Phase equilibria and thermodynamic properties in the Au–Sn system. *Gold Bulletin*, 36(2):39–50, 2003.

[5] N. Arikan and Ü. Bayhan. First-principles study of electronic and dynamic properties of AgMg and AgZn. *Solid State Communications*, 152(10):891–893, 2012. doi:10.1016/j.ssc.2012.02.009.

[6] M. Besterci and V. Prochazka. Electrical conductivity of internally oxidized Ag-Mg and Ag-Al alloys. *Soviet Powder Metallurgy and Metal Ceramics*, 14(2):169–172, 1975.

[7] R. H. Cui, Z. C. Dong, and C. G. Zhong. First principles investigation of structural, mechanical, dynamical and thermodynamic properties of AgMg under pressure. *Materials Research Express*, 4(12):126503, 2017. doi:10.1088/2053-1591/aa9c92.

[8] Y. Liu, R. G. Jordan, and S. L. Qiu. Electronic structures of ordered Ag-Mg alloys. *Physical Review B*, 49(7):4478–4485, 1994.

[9] S. S. Chouhan, G. Pagare, S. Sanyal, and M. Rajagopalan. First principles study on

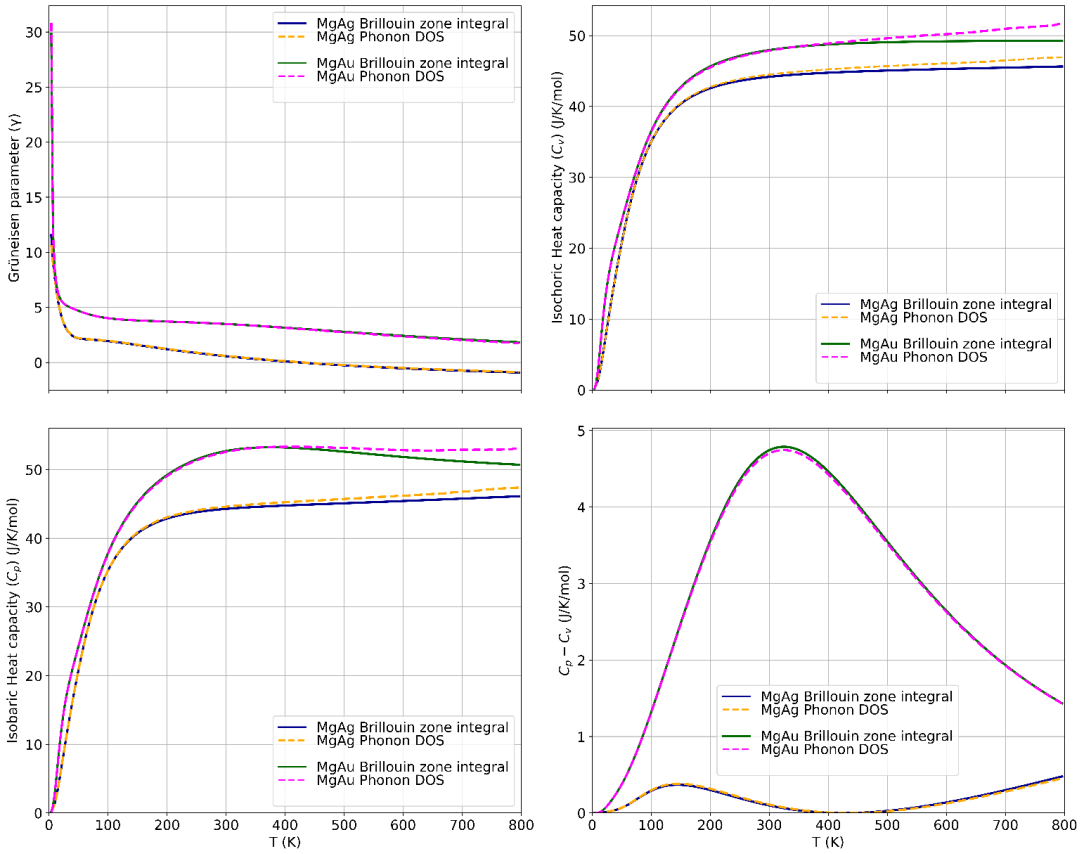

Figure 7: Variation of Grüneisen parameter, isochoric heat capacity (C_v), isobaric heat capacity (C_p), and their difference for MgAg and MgAu alloys as a function of temperature.

structural, electronic and elastic properties of AgX and AuX (X = Mg, Sc, Zn and Cd) intermetallic compounds. *Computational Materials Science*, 65:58–65, 2012.

[10] D. Liu, X. Dai, X. Wen, G. Qin, and X. Meng. Predictions on the compositions, structures, and mechanical properties of intermediate phases in binary Mg–X (X = Sn, Y, Sc, Ag) alloys. *Computational Materials Science*, 106:180–187, 2015.

[11] P. Giannozzi, O. Baseggio, P. Bonfà, et al. Quantum espresso toward the exascale. *Journal of Chemical Physics*, 152(15):154105, 2020. doi:10.1063/5.0005082.

[12] J. P. Perdew, K. Burke, and M. Ernzerhof. Generalized gradient approximation made simple. *Physical Review Letters*, 1996.

[13] X. Gong and A. Dal Corso. High-pressure and high-temperature thermoelectricity of tantalum: An ab initio study. *Journal of Chemical Physics*, 162(12), 2025. doi:10.1063/5.0258989.

[14] S. K. Yadav, S. Dahal, and B. Guragain. First principles calculations of mechanical, electronic, thermoelectric and thermal properties of ZnCu. *BIBECHANA*, 22(2):188–194, 2025. doi:10.3126/bibechana.v22i2.79223.

[15] S. K. Yadav, U. Chaudhary, and G. C. Kaphle. Exploring the structural, elastic, electronic, and optical properties of Na-based hydrides X_3NaH_4 (X= K, Rb) for hydrogen storage applications: A First-principles study. *International Journal of Hydrogen Energy*, 160:150637, 2025.

[16] U. Chaudhary, S. Chaudhary, D. K. Yadav, G. C. Kaphle, and S. K. Yadav. First-Principles Investigation of Structural, Elastic, Electronic, and Optical Properties of $AcMO_3$ (M= B, Sc) Perovskites. *physica status solidi (b)*, 262(5):2400574, 2025.

[17] B. Chettri, P. Karki, P. Chettri, S. K. Das, S. Das, and B. Sharma. Ab Initio Investigation of Optical and Electronic Properties of Pt-Doped Pentagonal $PdSe_2$ Monolayer. *physica status solidi (b)*, 261(3):2300335, 2024.

[18] B. Chettri, B. Sharma, S. K. Das, P. Chettri, P. Karki, and P. R. Bhutia. A First-Principle Investigation of Sc-Doped MoS_2 for Hydro-

gen Gas Detection. In *2024 IEEE International Conference of Electron Devices Society Kolkata Chapter (EDKCON)*, pages 567–572. IEEE, 2024.

[19] T. Ouahrani, F.-Z. Medjdoub, S. Gueddida, A. Lobato Fernandez, R. Franco, N.-E. Benkhettou, M. Badawi, A. Liang, J. Gonzalez, and D. Errandonea. Understanding the pressure effect on the elastic, electronic, vibrational, and bonding properties of the $CeScO_3$ perovskite. *The Journal of Physical Chemistry C*, 125(1):107–119, 2020.

[20] U. Chaudhary, G. C. Kaphle, and S. K. Yadav. Pressure-dependent structural, elastic, electronic, thermodynamic, and optical properties of $LuGaO_3$ perovskite: A first-principles study. *AIP Advances*, 15(8), 2025.

[21] S. K. Yadav, S. Dahal, R. Khadka, B. Guragain, P. Pokharel, P. Oli, and D. Adhikari. First Principles Study of Electronic, Vibrational, Elastic, and Thermodynamic Properties of Sc-X (X= P, S, Se) Compounds. *Engineering Reports*, 7(1):e13115, 2025.

[22] P. Pokharel, S. K. Yadav, N. Pantha, and D. Adhikari. Strain-dependent electronic, mechanical and piezoelectric properties of $ZrSiO_3$ 2D monolayer: A first principle approach. *Journal of Physics and Chemistry of Solids*, 193:112198, 2024.

[23] M. Jamal, S. J. Asadabadi, I. Ahmad, and H.A. R. Aliabad. Elastic constants of cubic crystals. *Computational Materials Science*, 95:592–599, 2014.

[24] G. Vaitheeswaran, V. Kanchana, S. Heathman, M. Idiri, T. Le Bihan, A. Svane, A. Delin, and B. Johansson. Elastic constants and high-pressure structural transitions in lanthanum monochalcogenides from experiment and theory. *Physical Review B—Condensed Matter and Materials Physics*, 75(18):184108, 2007.

[25] Z. Charifi, H. Baaziz, Y. Saeed, A. H. Reshak, and F. Soltani. The effect of chalcogen atom on the structural, elastic, and high-pressure properties of XY compounds (X= La, Ce, Eu, and Y= S, Se, and Te): An ab initio study. *physica status solidi (b)*, 249(1):18–28, 2012.

[26] A. Bouhemadou, R. Khenata, and M. Maamache. Structural phase stability and elastic properties of lanthanum monochalcogenides at high pressure. *Journal of Molecular Structure: THEOCHEM*, 777(1-3):5–10, 2006.

[27] F. Mouhat and F. Coudert. Necessary and sufficient elastic stability conditions in various crystal systems. *Physical review B*, 90(22):224104, 2014.

[28] M. Born and K. Huang. *Dynamical Theory of Crystal Lattices*. Springer-Verlag, Berlin, 1 edition, 1982.

[29] J. Puibasset. Grand potential, helmholtz free energy, and entropy calculation in heterogeneous cylindrical pores by the grand canonical monte carlo simulation method. *The Journal of Physical Chemistry B*, 109(1):480–487, 2005.

[30] V. N. Belomestnykh. The acoustical grüneisen constants of solids. *Technical Physics Letters*, 30(2):91–93, 2004.